Electrical Power and Energy Systems 165 (2025) 110463

Contents lists available at ScienceDirect

International Journal of Electrical Power and Energy Systems

journal homepage: www.elsevier.com/locate/ijepes

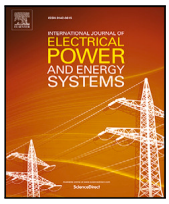

Hierarchical optimal frequency support scheme of wind farm with both grid-forming and grid-following wind turbines

Qihang Zong [a], Wei Yao [a,*], Hongyu Zhou [a], Yongxin Xiong [b], Wei Gan [c], Jinyu Wen [a]

[a] State Key Laboratory of Advanced Electromagnetic Engineering and Technology, School of Electrical and Electronic Engineering, Huazhong University of Science and Technology, Wuhan, 430074, China
[b] Department of Electrical and Electronic Engineering, The Hong Kong Polytechnic University, 999077, Hong Kong, China
[c] School of Engineering, Cardiff University, Cardiff CF24 3AA, United Kingdom

ARTICLE INFO

Keywords:
Wind farms
Frequency support
Grid-forming (GFM)
Grid-following (GFL)
Duality consistency

ABSTRACT

Renewable energy sources such as wind power have grown exponentially in recent years. Conventional grid-following wind turbines (GFL-WTs) run the risk of oscillations under weak grids. To operate stably over a wide range of grid strength, the hybrid wind farm with both grid-forming wind turbines (GFM-WTs) and GFL-WTs is an effective form. Due to the declining frequency stability of the renewable power system, it is important for wind farms to provide frequency support. However, effective frequency support control of such hybrid wind farm is a crucial issue. Hence, this paper proposes a hierarchical optimal frequency support (HOFS) scheme for the hybrid wind farm to optimize frequency support. Firstly, the system frequency response models of GFM-WTs and GFL-WTs are established for analysis and comparison. A duality consistency is revealed. In conclusion, the frequency support effects of GFM-WTs and GFL-WTs are consistent once both structures and parameters satisfy the revealed duality consistency formula. Secondly, a two-level HOFS scheme benefiting from the above analysis is designed. Level I is optimal frequency control of WT. Level II is coordination control of multiple WTs. The former level according to the duality consistency enables the GFM-WTs or GFL-WTs to optimally support the frequency, respectively. The latter level mitigates the additional frequency drop due to power limitation, particularly in high wind speed scenarios. Finally, case studies are undertaken on a two-area integration system with a wind farm. Both simulation and real-time experimental results verify the effectiveness of the HOFS scheme.

1. Introduction

As one of the important renewable energy sources to mitigate the global warming problem, wind power has grown rapidly in recent years [1–3]. However, the stable operation of wind farms (WFs) is challenging. Wind turbines (WTs) commonly adopt the grid-following (GFL) control in engineering. GFL-WTs are unstable under weak grids [4]. Thus, grid-forming (GFM) control has been proposed and received widespread attention in recent years. GFM-WTs significantly improve small-signal stability under weak grids [5,6]. Nevertheless, GFM-WTs have poor small-signal stability under strong grids while GFL-WTs are good instead. For operation over a wide range of short-circuit ratios (SCR), the hybrid WF with both GFM-WTs and GFL-WTs has become a new form of WF [7,8].

The integration of large-scale WTs poses a threat to the frequency stability of the power system [9]. Unlike the rotating mechanical structure of synchronous generators, WTs are connected to the power system through electric power inverters. Consequently, they cannot provide frequency support directly. That leads to a significant deterioration of the frequency security characteristics of the system [10]. Therefore, it is a critical requirement for the hybrid WF to be capable of frequency support according to the grid codes [11–13]. The better hybrid WF supports the frequency, the better it is for preventing frequency breakdown. However, there are two issues that need to be resolved regarding achieving frequency support for such hybrid WF. One is how to recognize the differences between GFL-WTs and GFM-WTs especially in terms of frequency support. The other is how to control the hybrid WFs specifically.

For the former issue, the comparison between GFL-WTs and GFM-WTs is expected and complex. GFL-WTs and GFM-WTs are regarded as controlled current sources and voltage sources, respectively [14,15]. GFL-WTs are typically characterized by the phase-locked loop (PLL) that follows the voltage phase of the grid [16,17]. For the GFM-WTs, they do not need the PLL structure. They establish the phase through the active power loop. Ref. [18] elaborates a pioneering duality

* Corresponding author.
E-mail address: w.yao@hust.edu.cn (W. Yao).

https://doi.org/10.1016/j.ijepes.2025.110463
Received 3 October 2024; Received in revised form 13 December 2024; Accepted 3 January 2025
Available online 14 January 2025

theory for GFL and GFM inverters, in terms of synchronization control, grid-interfacing characteristics, and swing characteristics. However, the GFL inverters in the above analysis do not consider the frequency support achieved by the additional loop. In terms of frequency support, Ref. [19] concludes that GFM inverters have better frequency peaks and nadirs compared to GFL inverters with frequency support. However, the relative advantage depends on the system parameters. Specifically, the weak support provided by GFL inverters is due to oscillations in [19]. In other words, the conclusion of the relative advantage in frequency support effectiveness is not general. In conclusion, the general comparison of their frequency support capabilities is lacking although both GFL-WTs and GFM-WTs are available to support frequency.

For the latter issue, the frequency support of the WF with only GFL-WTs or GFM-WTs has been investigated [20,21]. For the GFL-WF, the frequency support control is based on the collected frequency as input to generate additional active power. The additional power is attached to the reference of the maximum power point tracking (MPPT). Typical controls contain droop control [22], virtual inertia [23], and synthetic inertia control (SIC) [24,25] which is the combination of both. Cooperative frequency support of multiple WTs in a WF through communication is proposed in [26]. The GFM-WTs establish their own frequency and have independent frequency support capability. Typical controls include droop control [27] and virtual synchronous generator (VSG) control [28]. However, the above controls are designed to mimic the inertia and governor of the synchronous generator. It results in a failure to utilize the optimal support capability of the flexible control of the WTs, or it is non-optimal. Refs. [29,30] propose an optimal auxiliary frequency (OAF) control for WTs that achieves optimal frequency nadir by constructing and solving an optimization model for WF participation in system frequency regulation. The OAF control coordinates the power characteristics of the WTs and the synchronous generator at different stages. Nevertheless, the nature of OAF control is applicable to GFL-WTs. It cannot be applied directly to the hybrid WF. In addition, the power limitations of the WTs should be taken into account in high wind speed scenarios.

To solve these issues, this paper analyzes the frequency support mechanisms of GFM-WTs and GFL-WTs, respectively. The system frequency response (SFR) models are established to compare their frequency support capabilities for general conclusions rather than special cases. Benefiting from the comparison analysis, a hierarchical optimal frequency support (HOFS) scheme of the hybrid WF is proposed to achieve optimal frequency support over a wide range of grid strength. Compared with the OAF control proposed in [30], the HOFS scheme has significantly improved frequency support at high wind speeds and has a wider safe operation region of grid strength. In addition, the effectiveness and advantages of the scheme are verified in the test system. The main contributions of this paper are as follows:

- A hierarchical optimal frequency support (HOFS) scheme for the hybrid WF with both GFM-WTs and GFL-WTs is proposed to optimize frequency support. The design in Level I of the HOFS scheme results in optimal frequency support of GFM-WT and GFL-WT, considering the characteristics of the frequency decline and speed recovery periods. Level II coordinates multiple WTs to achieve optimal support of the whole hybrid WF. Compared to other controls such as SIC, VSG, and OAF [30], the HOFS scheme results in a better frequency nadir of the system frequency after disturbance events. In addition, the HOFS scheme enables optimal frequency support over a wider range of grid strengths.
- The frequency response models GFM-SFR and GFL-SFR are developed for comparison by analyzing their respective frequency support processes of GFM $\Delta P \rightarrow \Delta f$ and GFL $\Delta f \rightarrow \Delta P$. Further, a duality consistency is revealed. It is concluded that the frequency support effects of GFM-WTs and GFL-WTs are consistent once both structures and parameters satisfy the revealed duality consistency formula. As a result, the optimal frequency support structure of GFM-WT can be obtained from that of GFL-WT. The duality consistency allows both types of WTs to achieve optimal frequency support in Level I.
- The power interaction factor is designed for the coordination of multiple WTs in Level II. It mitigates the additional drop in frequency due to power limitations in high wind speed scenarios. That contributes to the WF frequency support using the HOFS scheme applicable to the constant speed zone of the WTs in addition to the MPPT zone.

The rest of the paper is organized as follows. Section 2 proves the duality consistency of the GFM-WTs and GFL-WTs in terms of frequency support. In Section 3, the proposed HOFS scheme is presented. Section 4 is the validation of the proposed theory and scheme. Section 5 concludes the paper.

2. Duality consistency analysis for frequency support of GFM and GFL wind turbines

2.1. Mechanisms of GFM-WTs and GFL-WTs for frequency support

The mechanisms of GFM-WTs and GFL-WTs to participate in the frequency regulation of the system are different, although they both utilize rotor energy to regulate the output active power. The frequency support control structures of the GFM-WT and GFL-WT in synchronous dq frame are shown in Fig. 1. For the GFM-WTs, the active power loop outputs the phase θ. This loop has both synchronization and frequency support functions. In particular, the process of active power deviation ΔP to frequency deviation Δf is the key to frequency support. For the GFL-WTs, the PLL follows the grid voltage and outputs the phase θ, specifically for synchronization. The further frequency deviation Δf obtained through the PLL generates additional power increment ΔP. The process of $\Delta f \rightarrow \Delta P$ is the key to frequency support. The GFM-WTs and GFL-WTs are simplified into aggregated models for analysis and comparison. The roles of these two physical processes are as follows:

- $\Delta P \rightarrow \Delta f$ *process of GFM-WTs*: The output active power deviation ΔP between actual and reference of the WT is used to autonomously regulate its frequency. Further, this leads to frequency deviation Δf of the WT. As a result, the phase of the point of common coupling (PCC) is shifted. In addition, the WTs adjust the active power delivered to the integrated system due to phase differences. Eventually, the frequencies of the interconnected systems are the same and supported.
- $\Delta f \rightarrow \Delta P$ *process of GFL-WTs*: The frequency deviation Δf of the system followed by the PLL is utilized to regulate the active power of WTs. Further, this results in an additional active power increment ΔP for the WT. The additional output active power is able to reduce the power shortage in the synchronous system. Thus, the frequency of the system is supported.

2.2. Dual SFR models of GFM-WTs and GFL-WTs

The SFR model simplifies the complexity of frequency analysis, which is a typical method [3]. Although it is not the most detailed representation, it provides sufficiently high accuracy for the electromechanical transients in wind-integrated systems [10,31]. According to the above dual frequency regulation participation processes, this paper establishes the SFR models of GFM-WTs and GFL-WTs supporting system frequency respectively to analyze the frequency responses. They are used to analyze the frequency characteristics under power disturbance.

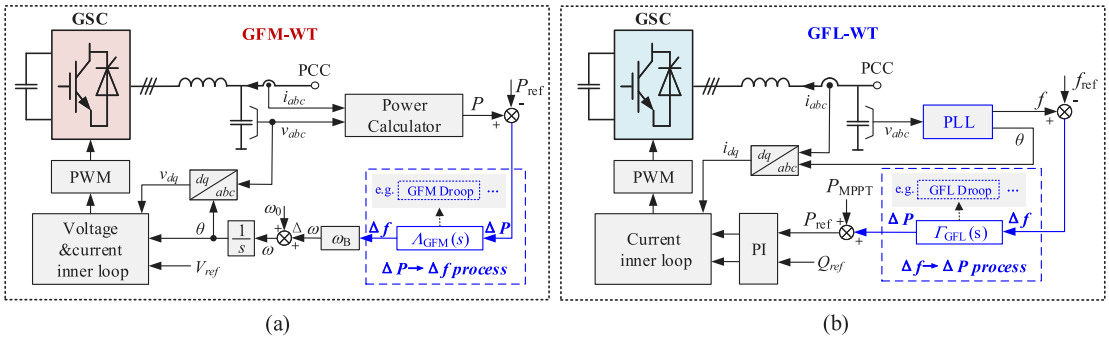

Fig. 1. Frequency support control structures of grid-forming and grid-following wind turbines in synchronous dq frame. (a) Grid-forming wind turbine with frequency support control. (b) Grid-following wind turbine with frequency support control.

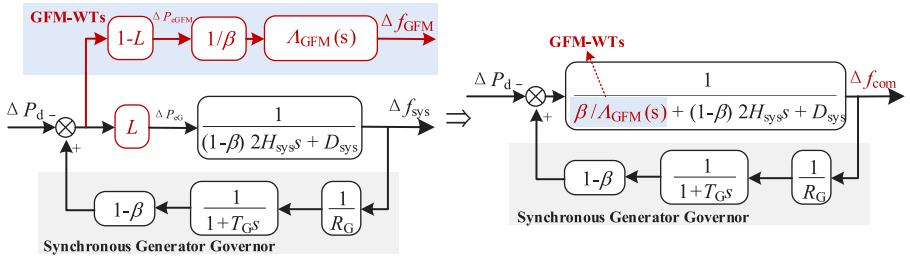

Fig. 2. SFR models of the GFM-WTs engaged in system frequency regulation. (a) Proposed original GFM-SFR model. (b) Equivalent GFM-SFR model.

2.2.1. GFM-SFR model

The $\Delta P \rightarrow \Delta f$ process design of the GFM-WTs determines the frequency response characteristics. The different designs of it significantly affect the effectiveness of the frequency support.

$$\Delta f_{\mathrm{GFM}}(s) = \Lambda_{\mathrm{GFM}}(s)\Delta P_{\mathrm{GFM}}(s) \tag{1}$$

where, Δf_{GFM} and ΔP_{GFM} are the frequency deviation and active power deviation of GFM-WTs. $\Lambda_{\mathrm{GFM}}(s)$ represents the transfer function of the process, which is usually designed as droop or VSG, etc.

The GFM-WTs and synchronous generators respond to the electrical power shortage together. Therefore, the original GFM-SFR model is obtained as shown in Fig. 2(a). β is the penetration rate of the WTs. L is used to represent the ratio of the synchronous generators to regulate the shortage, which is difficult to determine due to the dynamic active power flow between them. H_{sys} and D_{sys} are the inertia and damping parameters of the synchronous system. Δf_{sys} is the frequency deviation of the synchronous system. ΔP_{d} is an active power disturbance in the system. R_{G} and T_{G} are the regulation coefficient and time constant of the equivalent synchronous generator governor.

The frequency deviation established by the GFM-WTs and the synchronous system frequency deviation have a common-mode component Δf_{com} and a differential-mode component Δf_{diff} of each [32,33].

$$\begin{cases} \Delta f_{\mathrm{GFM}} = \Delta f_{\mathrm{com}} + \Delta f_{\mathrm{diff},1} \\ \Delta f_{\mathrm{sys}} = \Delta f_{\mathrm{com}} + \Delta f_{\mathrm{diff},2} \end{cases} \tag{2}$$

where, Δf_{com} is the common-mode frequency deviation. $\Delta f_{\mathrm{diff},1}$ and $\Delta f_{\mathrm{diff},2}$ are the differential-mode deviations.

The differential-mode frequency deviations are minor and progressively declining. Consequently, the common-mode frequency deviation Δf_{com} is the most dominant component. Since the open-loop functions of Δf_{com} for the GFM-WTs and the system are equal, L can be derived as follows:

$$L = \frac{[(1-\beta)2H_{\mathrm{sys}}s + D_{\mathrm{sys}}]\Lambda_{\mathrm{GFM}}(s)}{\beta + [(1-\beta)2H_{\mathrm{sys}}s + D_{\mathrm{sys}}]\Lambda_{\mathrm{GFM}}(s)} \tag{3}$$

Therefore, the equivalent GFM-SFR model shown in Fig. 2(b) is obtained by taking Eq. (3) into the transfer function of the original model. The closed-loop transfer function Φ_{GFM} of the Δf_{com} with respect to the power disturbance ΔP_d is obtained:

$$\Phi_{\mathrm{GFM}}(s) = \underbrace{\frac{1}{(1-\beta)[2H_{\mathrm{sys}}s + D_{\mathrm{sys}} + 1/(1+T_{\mathrm{G}}s)R_{\mathrm{G}}]}}_{\text{Contribution of the synchronous generator}} + \underbrace{\beta/\Lambda_{\mathrm{GFM}}(s)}_{\text{GFM-WTs}} \tag{4}$$

From Eq. (4), the frequency response is divided into two parts. These are the contributions of the synchronous generators and GFM-WTs.

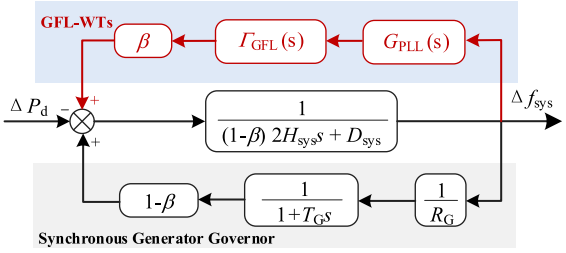

Fig. 3. SFR model of the GFL-WTs engaged in system frequency regulation.

2.2.2. GFL-SFR model

The $\Delta P \rightarrow \Delta f$ process of the GFL-WTs is also the focus of the frequency support. $\Gamma_{\mathrm{GFL}}(s)$ denotes the transfer function of the process. Restricted by the structure of the GFL control, $G_{\mathrm{PLL}}(s)$ is an extra session to represent the dynamic process of the PLL.

$$\Delta P_{\mathrm{GFL}}(s) = \underbrace{\frac{K_{\mathrm{P}}\omega_0 s + K_{\mathrm{I}}\omega_0}{T_{\mathrm{F}}s^3 + s^2 + K_{\mathrm{P}}\omega_0 s + K_{\mathrm{I}}\omega_0}}_{G_{\mathrm{PLL}}(s)} \Gamma_{\mathrm{GFL}}(s)\Delta f(s) \tag{5}$$

where, K_{P} and K_{I} are the PI parameters of the PLL. ω_0 is the base electrical angular velocity. T_{F} is the filter time constant for estimating the frequency derivative.

Further, the GFL-SFR model is obtained as shown in Fig. 3. Thus, the closed-loop transfer function Φ_{GFL} of Δf_{sys} with respect to ΔP_d is given by:

$$\Phi_{\mathrm{GFL}}(s)=\underbrace{\frac{1}{(1-\beta)[2H_{\mathrm{sys}}s+D_{\mathrm{sys}}+1/(1+T_{\mathrm{G}}s)R_{\mathrm{G}}]}}_{\text{Contribution of the synchronous generator}}+\underbrace{\beta G_{\mathrm{PLL}}(s)\Gamma_{\mathrm{GFL}}(s)}_{\text{GFL-WTs}} \tag{6}$$

The contribution of synchronous generators and that of GFL-WTs jointly affect the frequency response.

2.3. Duality consistency of frequency support

The effect of the respective participation of GFM-WTs and GFL-WTs in the system frequency support has been analyzed above. In particular, there are some reasonable assumptions and justifications for the analysis:

- The effects of voltage fluctuations are ignored while the dynamic relationship between frequency and active power is the only concern. This is because the voltage fluctuations are minimal in the system with only active disturbances and their effect on the frequency is indirect.
- The dynamic responses of the inner loops are ignored since the time scale of the frequency support concerned is much longer than the inner-loop response time.
- The differential-mode frequency components among different nodes are ignored since their values are minor and progressively declining.

According to Eqs. (4) and (6), the frequency support characteristics are satisfied:

$$\Phi_{\mathrm{GFM}}(s)=\Phi_{\mathrm{GFL}}(s),\ \text{if}\ \Lambda_{\mathrm{GFM}}(s)G_{\mathrm{PLL}}(s)\Gamma_{\mathrm{GFL}}(s)=1 \tag{7}$$

The duality consistency is revealed. It is concluded that the frequency support effects of GFM-WTs and GFL-WTs are consistent once the transfer function dual relationship is satisfied as Eq. (7). In other words, GFM-WTs and GFL-WTs have the same frequency support effectiveness as long as their structures and parameters are dual. Moreover, the response time of PLL is typically less than 200 ms, which is significantly shorter compared to the frequency support time of about 30 s. Consequently, the duality consistency formula can be simplified to $\Lambda_{\mathrm{GFM}}(s)=1/\Gamma_{\mathrm{GFL}}(s)$ by ignoring the PLL dynamic. It unifies the GFM-WTs and GFL-WTs in general regardless of the various structures.

3. Hierarchical optimal frequency support scheme of the hybrid wind farm

This section elaborates on how to control hybrid WFs for frequency support. In this paper, the optimal frequency support objective is a combination of the frequency nadir $\Delta f_{\min}$ and the frequency average. The objective is consistent with that in [30]. The nadir and average of frequency are combined by the coefficient η. It can be expressed as:

$$\max_{G_{\mathrm{WF}}}\quad\left(\Delta f_{\min}+\eta\cdot\frac{1}{t_{end}-t_0}\int_{t_0}^{t_{end}}\Delta f(t)\mathrm{d}t\right) \tag{8}$$

Based on the frequency response model of the system, the trajectory optimization model is constructed to solve numerically for the discrete points in the time domain. The optimal frequency transfer function for the system is obtained by fitting the time-domain solution.

$$G_{sys}(s)=\frac{1}{H_{\mathrm{G}}s-G_{\mathrm{WF}}(s)+K_{L,f}+\frac{K_{\mathrm{G,f}}}{1+sT_{\mathrm{G}}}}=\frac{1}{D_{sys}+2H_{sys}s} \tag{9}$$

where, H_{G}, T_{G}, $K_{\mathrm{G},f}$, $K_{L,f}$, D_{sys}, H_{sys} are the system frequency regulation parameters. The power transfer function of the wind farm G_{WF} can be solved.

The design is to keep the frequency at the nadir for a long time rather than having a significant trough. However, it is applicable only to conventional GFL-WFs. To enable optimal frequency support in the hybrid WF containing both GFM-WTs and GFL-WTs, the optimal frequency support for GFM-WTs is developed in this paper. Its core is the extension of the optimal frequency support from GFL-WT to GFM-WT through the revealed duality consistency formula, as $\Lambda_{\mathrm{GFM}}(s)=1/\Gamma_{\mathrm{GFL}}(s)$. The designed concept of frequency support controls for GFM-WT and GFL-WT is shown in Fig. 4. In addition to the frequency support control for individual GFM-WT or GFL-WT, coordination control for multiple WTs has also been designed. The proposed frequency control scheme is detailed in this section.

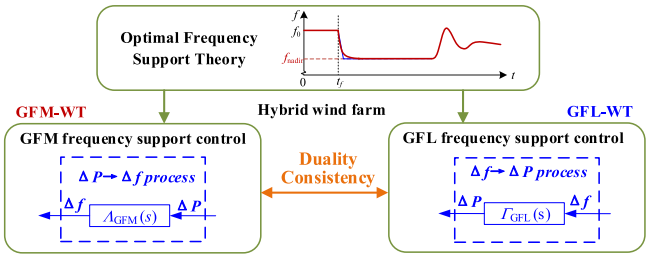

Fig. 4. Hybrid wind farm control design based on the revealed duality consistency and optimal frequency support theory.

3.1. Overview framework of HOFS scheme

The hybrid WF with both GFL-WTs and GFM-WTs can operate stably over a wide range of grid strength. Benefiting from the revealed duality consistency of GFM-WTs and GFL-WTs, a hierarchical optimal frequency support (HOFS) scheme of the hybrid WF is proposed for optimal frequency support over a wide range of grid strength. The HOFS scheme consists of two levels as shown in Fig. 5. Level I is optimal frequency control of WT. Level II is coordination control of multiple WTs. The former level allows individual WT to optimally support the frequency either as a GFM-WT or GFL-WT. The latter level enhances the frequency support capability of the WF in high wind speed scenarios through coordination. Moreover, the HOFS scheme is applicable to the constant speed zone in addition to the MPPT zone of WTs. The details are as follows:

3.1.1. Level I: Optimal frequency control of WT

For the GFM-WTs in the WF, GFM optimal frequency support control is employed. Meanwhile, the GFL optimal frequency support control is used for the GFL-WTs. The two controls are designed to satisfy $\Lambda_{\mathrm{GFM}}(s)=1/\Gamma_{\mathrm{GFL}}(s)$ based on the duality consistency revealed.

- *GFM optimal frequency support control.* It contains two stages. Stage I is the frequency decline support in the first period of transient, which is critical for the nadir. Stage II is the recovery stage in the later period of transient. The switching of the two stages is carefully designed.
- *GFL optimal frequency support control.* Similar in components to the GFM control, it also contains two stages of frequency decline support and recovery. However, it requires PLL to collect the f and generate θ.

3.1.2. Level II: Coordination control of multiple WTs

Distributed coordination control is designed. It generates interaction factor x_i for power coordination among WTs. Each WT gains an additional power value through the received factors. That allows the power shortage due to WT limitation to be compensated by the other WTs, preventing an extra frequency drop. It is suitable for all GFM-WTs and GFL-WTs in the WF.

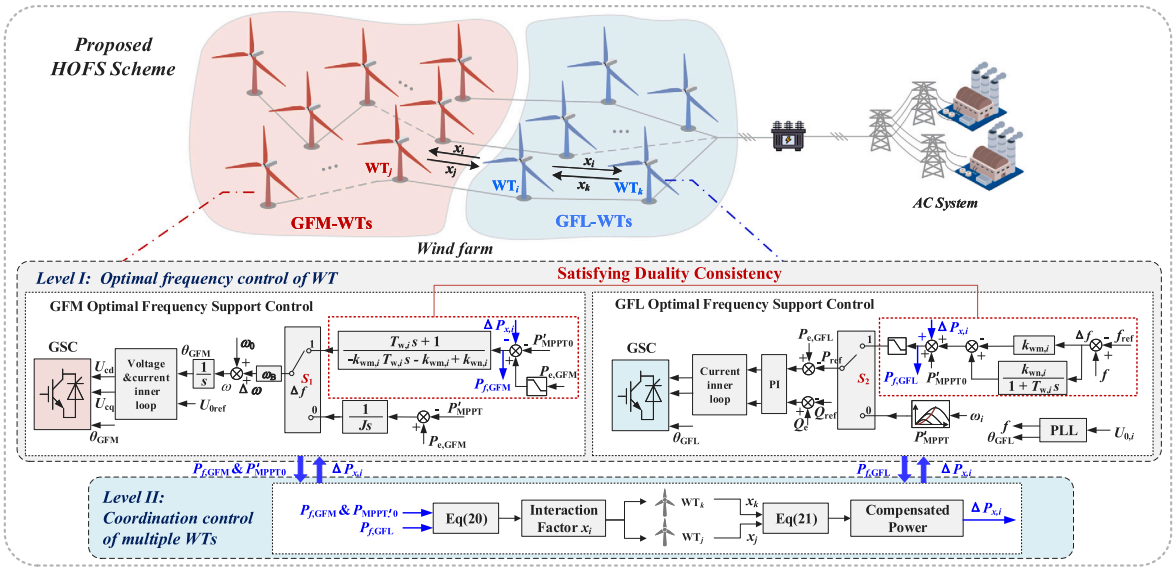

Fig. 5. The framework of proposed hierarchical optimal frequency support (HOFS) scheme for the hybrid WF with GFM-WTs and GFL-WTs.

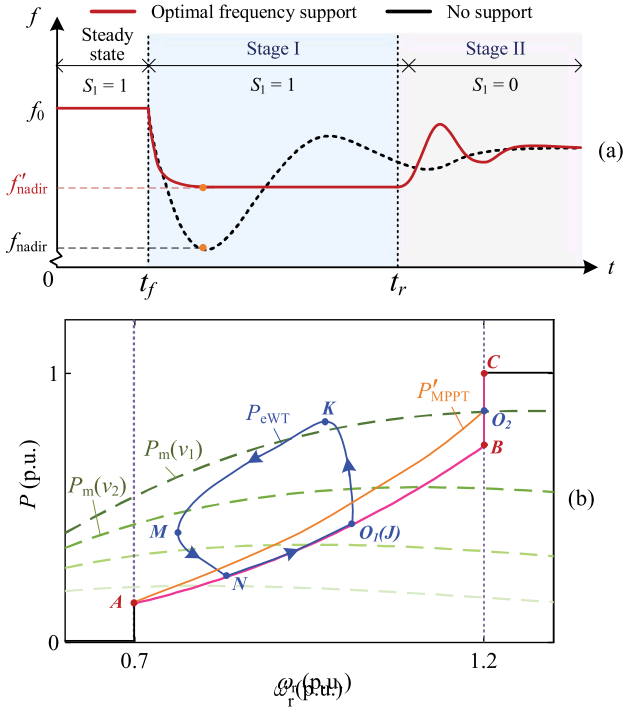

Fig. 6. Operating trajectories of the WT with optimal frequency support. (a) Frequency response trajectory. (b) Electromagnetic power and rotor speed trajectories.

3.2. GFM optimal frequency support control

The optimal frequency support claimed in this paper refers to the control that enables optimal frequency nadir f_{nadir} for WF integration with the system containing synchronous generators. The rotor speed of each WT will be restored to the original state after the transient. The proposed GFM optimal frequency support contains two stages. The control structure and the operation trajectories are shown in Figs. 5 and 6. In particular, the proposed control covers the MPPT zone and the constant speed operation zone of WT. The β of the SFR model in Section 2 is normalized to other parameters.

3.2.1. Stage I: Frequency decline support

The frequency begins to decline when there is a sudden active power shortage in the system. In the following, the mechanism of optimal frequency support of the GFM-WF to the connected system is analyzed in terms of the periods of the frequency response to capitalize on flexibility.

- *Inertial response period.* The synchronous generators provide inertia and the frequency declines approximately linearly. The WTs output as little power as possible to induce a widening of the frequency gap in order to motivate more primary frequency regulation output from the synchronous generators. Therefore, GFM-WTs are able to pull the system frequency down during this period by rapidly decreasing the $f_{\text{GFM},i}$ via a one-order response.
- *Bridging period.* The power of the primary frequency regulation of the synchronous generator increases very slowly due to physical factors such as the steam door opening. However, the inertia power has been reduced. This period is the key to the f_{nadir}. The GFM-WTs should reduce the f_{GFM} fluctuation in order to quickly output power to compensate for the power variation of the governor.
- *Primary frequency regulation period.* The f_{GFM} of the GFM-WTs continues to remain constant and its output power levels off.

The OAF control of GFL-WTs is equipped as a proportional segment and an inertial segment [30]. Based on the duality consistency of GFM-WTs and GFL-WTs for frequency support proposed in this paper, the control of the GFM-WTs in this stage is constructed:

$$\Lambda_{\text{GFM,OAF}i}(s) = \frac{\Delta f_{\text{GFM},i}(s)}{\Delta P_{\text{GFM,I}i}(s)} = \frac{T_{\text{w},i}s + 1}{-k_{\text{wm},i}T_{\text{w},i}s - k_{\text{wm},i} + k_{\text{wn},i}} \tag{10}$$

$$\Delta P_{\text{GFM,I}i} = P_{\text{eGFM},i} - P'_{\text{MPPT0}} - \Delta P_{\text{x},i} \tag{11}$$

where, $\Lambda_{\text{GFM,OAF}i}$ is the $\Delta P \rightarrow \Delta f$ transfer function of the i-th GFM-WT in Stage I. $T_{\text{w},i}$, $k_{\text{wm},i}$ and $k_{\text{wn},i}$ are the optimal support parameters. P'_{MPPT0} is the initial power of frequency regulation. $P_{\text{eGFM},i}$ is the electromagnetic power of the GFM-WT. $\Delta P_{\text{x},i}$ is the additional coordination power of Level II.

As analyzed above, the essential cause of the f_{nadir} is the governor limited by physical factors. The optimal support control for the WF is to patch it up in the weak bridging period. It is characterized by a rapid reduction of the frequency to its minimum value and keeping it constant.

3.2.2. Stage II: Rotor speed recovery

The frequency support of WT utilizes the temporary kinetic energy of the rotor. It is short term and the rotor speed needs to be restored to its original state for continuous operation. This stage should make the electromagnetic power of the WT lower than the mechanical power, so the rotor accelerates. The design concept of the recovered control is as follows. One is that the WT can naturally recover to the initial point if the electromagnetic power output is in accordance with the MPPT curve. The second is that the GFM frequency transfer function adopts the non-differential regulation to reduce the power deviation as soon as possible, which allows the WT power to be output better according to the preset curve. Based on this, the designed GFM $\Delta P \rightarrow \Delta f$ transfer function for the stage is:

$$\Lambda_{\mathrm{GFM,R}i}(s) = \frac{\Delta f_{\mathrm{GFM},i}(s)}{\Delta P_{\mathrm{GFM,II}i}(s)} = \frac{1}{Js} \tag{12}$$

$$\Delta P_{\mathrm{GFM,II}i} = P_{\mathrm{eGFM},i} - P'_{\mathrm{MPPT}} \tag{13}$$

where, J is the inertia coefficient. P'_{MPPT} is the improved MPPT curve.

It is worth noting that the proposed control of the WT contains the MPPT zone (A-B) and the constant speed zone (B-C), as shown in Fig. 6(b). Speed recovery of the constant speed zone is difficult due to the fact that the same speed corresponds to different power values. Therefore, P'_{MPPT} is specially designed to be used for the speed recovery stage.

$$P'_{\mathrm{MPPT}} = k_{\mathrm{opt}}\omega_{r,i}^3 + \frac{P(O_2) - k_{\mathrm{opt}}\omega_{r,\max}^3}{\omega_{r,\max} - \omega_{r,\min}} k_1(\omega_r - \omega_{r,\min}) \tag{14}$$

where, k_{opt} is the conventional MPPT curve constant coefficient. $P(O_2)$ is the initial power located in the constant speed zone. k_1 is the zone sign coefficient, $k_1 = 0$ for the MPPT zone and $k_1 = 1$ for the constant speed zone. $\omega_{r,i}$ is the rotor speed of the i-th WT. $\omega_{r,\max}$ and $\omega_{r,\min}$ the maximum and minimum limits of rotor speeds.

3.2.3. Switching of stages

The trajectories of the WT with optimal frequency support are shown in Fig. 6. There is a sudden load increase at $t = t_f$, and the deviation of electrical angular velocity from the set value exceeds the dead zone. Therefore, the WT enters Stage I. Its electromagnetic power curve is $O_1 - K - M - N$, as shown in Fig. 6(b). Switch $S_1 = 1$ at both steady state and Stage I. When $t = t_r$, the electromagnetic power is less than P'_{MPPT} or the speed is less than the minimum speed $\omega_{\min}$. At that moment, Stage I switches to Stage II. The electromagnetic power curve of Stage II is $N - J$. The logic of switch S_1 is:

$$\begin{cases} S_1 = 0, \ \Delta\omega_i > \Delta\omega_{db} \ \&(P_{\mathrm{eGFM},i} < P'_{\mathrm{MPPT},i} | \omega_{r,i} \le \omega_{\min}) \\ S_1 = 1, \ \text{else} \end{cases} \tag{15}$$

where, $\Delta\omega_i$ is the electrical angular velocity deviation of the i-th WT. $\Delta\omega_{db}$ is the dead zone of electrical angular velocity.

3.3. GFL optimal frequency support control

The GFL optimal frequency support also contains two stages, whose control structure and operation trajectory are shown in Figs. 5 and 6. The control proposed in this paper additionally broadens the applied field to the constant speed zone as compared to OAF in [30]. In addition, the control parameters are calibrated more carefully and conveniently rather than by trial and error.

3.3.1. Stage I: Frequency decline support

Frequency optimal support is realized by adjusting the active power reference value derived from the Δf. The control structures of GFM-WTs and GFL-WTs in Stage I are dual. The designed GFL $\Delta f \rightarrow \Delta P$ transfer function in Stage I is:

$$\Gamma_{\mathrm{GFL,OAF}i}(s) = \frac{\Delta P_{\mathrm{GFL,OAF}i}(s)}{\Delta f(s)} = -k_{\mathrm{wm},i} + \frac{k_{\mathrm{wn},i}}{1 + T_{\mathrm{w,i}}s} \tag{16}$$

$$P_{\mathrm{ref,I}i} = \Delta P_{\mathrm{GFL,OAF}i} + P'_{\mathrm{MPPT0}} + \Delta P_{\mathrm{x},i} \tag{17}$$

where $P_{\mathrm{GFL,OAF}i}$ is the active deviation of the i-th GFL-WT in Stage I.

3.3.2. Stage II: Rotor speed recovery

The speed recovery of GFL-WT is easily achieved by only changing the active power reference value. Stage II control is designed as:

$$P_{\mathrm{ref,II}i} = P'_{\mathrm{MPPT0}} \tag{18}$$

3.3.3. Switching of stages

The switching thresholds for Stage I and Stage II are equally t_r and point N as shown in Fig. 6. The logic of switch S_2 is designed:

$$\begin{cases} S_2 = 1, \ \Delta f > \Delta f_{db} \\ S_2 = 0, \ P_{\mathrm{eGFL},i} < P'_{\mathrm{MPPT},i} \mid \omega_{r,i} \le \omega_{\min} \end{cases} \tag{19}$$

where Δf_{db} is the frequency regulation dead zone.

3.3.4. Setting of critical control parameters

The parameters setting for GFM and GFL optimal controls are the same due to their consistency. The three control parameters of Stage I are required to be carefully designed. They determine whether the frequency can be kept smooth at the nadir. The sum of $k_{\mathrm{wm},i}$ and $k_{\mathrm{wn},i}$ for each turbine is $k_{\mathrm{wm,sum}}$ and $k_{\mathrm{wn,sum}}$, respectively. $k_{\mathrm{wn,sum}}$ is valued as $1/R_{\mathrm{G}}$. The time coefficient $T_{\mathrm{w},i}$ is equal to the T_{G} of the aggregated governor. Their setting takes into account the actual frequency regulation capability of the different WTs.

$$\begin{cases} E_i = \dfrac{\omega_{r,i}^2 - \omega_{r,\min}^2}{\omega_{r,\max}^2 - \omega_{r,\min}^2} \\ k_{\mathrm{wm},i} = \dfrac{E_i}{\sum_{i=1}^{N} E_i} k_{\mathrm{wm,sum}} \\ k_{\mathrm{wn},i} = \dfrac{E_i}{\sum_{i=1}^{N} E_i} k_{\mathrm{wn,sum}} \end{cases} \tag{20}$$

where E_i denotes the energy factor that can be utilized by each WT.

A larger $k_{\mathrm{wm,sum}}$ enables maximum rotor kinetic energy and better supports the frequency. However, a too large value will result in rotor speed protection. The scenario for $k_{\mathrm{wm,sum}}$ setting is to set the common maximum load disturbance ΔP_d in standard operating condition. Actually, $k_{\mathrm{wm,sum}}$ is the expected value when the rotor speed at M is equal to $\omega_{\min}$. The time-domain expression for the ω_r is solved by Eq. (21). Thus, $k_{\mathrm{wm,sum}}$ is available by bringing $M(\omega_{\min}, P_{mM})$ into it.

$$\begin{cases} f(s) = \dfrac{\Delta P_d}{s\left(D_{\mathrm{sys}} + k_{\mathrm{wm,sum}} + 2H_{\mathrm{sys}}s\right)} \\ P_{e\mathrm{WT}}(s) = -\left(k_{\mathrm{wm,sum}} - \dfrac{k_{\mathrm{wn,sum}}}{T_{\mathrm{w}}s + 1}\right) f(s) \\ P_{m\mathrm{WT}}(s) = K_{Pm}\omega_r(s) \\ \omega_r(s) = \dfrac{P_{m\mathrm{WT}}(s) - P_{e\mathrm{WT}}(s)}{2H_{\mathrm{w}}} \end{cases} \tag{21}$$

where, H_{w} is the intrinsic inertia of WT. K_{Pm} is the slope of the linearized MPPT curve. $P_{m\mathrm{WT}}$ and $P_{e\mathrm{WT}}$ are the mechanical and electromagnetic power of WT, respectively.

3.4. Coordination control of multiple WTs

There is a problem in the frequency support that the expected output power is limited due to the capacity limitation of the converter. It often occurs in WTs with high initial power, especially those operating in the constant speed zone. The expected but over-limit power is prohibited in order to protect the converter. As a result, an extra frequency drop occurs at Stage I. The f_{nadir} is lower than that expected as shown in Fig. 7. Coordination control is designed to solve the problem. Its core is the augmentation of the power shortage due to limitation by the unsaturated WTs through the power interaction factor x_i. This control is applicable to all GFM and GFL units in the WF. The

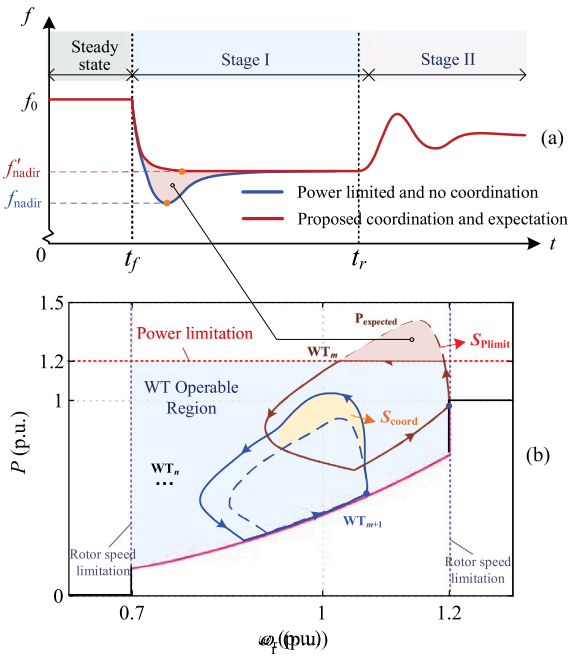

Fig. 7. Trajectories of frequency support with coordination. (a) Frequency response trajectories. (b) Electromagnetic power and rotor speed trajectories.

expression for x_i is:

$$x_i = \begin{cases} P_{f,\mathrm{GFM}} + P'_{\mathrm{MPPT0}} - P_{\max}, & P_{f,\mathrm{GFM}} + P'_{\mathrm{MPPT0}} > P_{\max} \\ P_{f,\mathrm{GFL}} - P_{\max}, & P_{f,\mathrm{GFL}} > P_{\max} \\ 0, & else \end{cases} \tag{22}$$

where $P_{f,\mathrm{GFM}}$ and $P_{f,\mathrm{GFL}}$ are the specific power values for the GFM and GFL optimal controls respectively in Fig. 5.

In this paper, the Jensen's Model is used to describe the wake effect [34,35]. Detailed formulas of wake effect are as Appendix. The wake effects of wind speeds are expressed as different active powers. That is because the WTs all utilize MPPT control, as shown in Eq. (23). Specifically, each WT has a different P'_{MPPT0}. The $P_{f,\mathrm{GFL}}$ of the GFL-WT includes P'_{MPPT0} and transient added power. In the control of multiple WTs, the different WTs' powers are coordinated through power interaction factors. Therefore, the wake effect is fully considered in the control of multiple WTs.

$$P_{\mathrm{MPPT0},i} = \frac{1}{2}\pi\rho R^2\left(c_0 - \frac{c_1^2}{4c_2}\right)V_i^3 = k_{\mathrm{opt}}V_i^3 \tag{23}$$

where, c_0, c_1, c_2, ρ are constants and V_i is the wind speed of the ith WT considering the wake effect.

The additional power generated of each WT by receiving interaction factors is:

$$\Delta P_{x,i} = (x_k + x_j)/2 \tag{24}$$

Although the two objects that the WT interaction factor is passed to are determined by the actual topology, the effect is still realizable. As shown in Fig. 7, the medium power WTs compensate S_{coord} for the expected power P_{expected} that the high power WTs cannot generate. Thus the frequency support is enhanced.

4. Case studies

The analyses are based on the actual WF engineering parameters in a province in Northwest China. A WF connected to the IEEE two-area system as shown in Fig. 8 is established on the MATLAB/Simulink

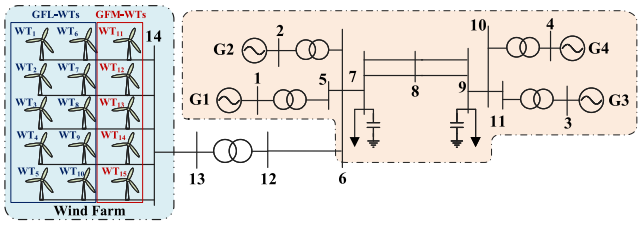

Fig. 8. Test model of the IEEE 2-area integration system with a wind farm.

and Opal-RT real-time simulation platform using the MatPSST toolbox [36]. The WF consists of 15 equivalent WTs, etc., and each WT is assembled by 20 direct-drive turbines with 3.33 MW. The installed wind power penetration is 37.7%. The total active load of the system is 2654.5 MW.

To validate the analysis and control described in this paper, the following distinction of validation is made. WTs 11~15 are the GFM units. And the other WTs are GFL units. Notably, the proportion of GFM-WTs in practical applications is discussed by several frontier studies [7,37]. It was concluded that a percentage of about 20%–45% can already increase the stability margin significantly. The number of GFM-WTs in this paper is based on the above findings. Therefore, the setting of 5 out of 15 turbines as GFM-WTs (33%) is suitable for practical applications.

The sub-item and overall proposed HOFS schemes addressed below are shown in Table 1 to verify the effects of the scheme in parts. All WTs of the WF in Sections 4.1 and 4.2 are set to the same including control type and status. The purpose is to purely validate the effect of the GFM control without the influence of the partly GFL control. The complete HOFS scheme is applied in Sections 4.3 and 4.4. In addition, wake effects [38,39] of the WF by wind are considered.

4.1. Duality consistency verification of GFM and GFL wind turbines

In this subsection, a 300 MW load increase occurs at $t = 5$ s on bus 7 of the system. It is worth noting that the focus of the proposed GFM and GFL duality consistency is on Stage I of the transient. Therefore, the Stage II of recovery is not considered in the validation of this subsection. In addition, all WTs are in the same state for better comparison. Cases are given to compare the frequency support of the three typical and proposed controls. Fig. 9 illustrates the control structures of GFM-WTs and GFL-WTs for verification.

4.1.1. Case1: Droop control of GFL vs. droop control of GFM

The results of the system frequency and the rotor speeds of the WTs are shown in Fig. 10(a) and (b). The GFL droop parameter $K_{p,\mathrm{GFL}}$ is taken to be the values of 20, 50, and 80, respectively. At the same time, the GFM droop parameter $K_{p,\mathrm{GFM}}$ is taken to be the inverse of $K_{p,\mathrm{GFL}}$. The analysis and results show that the frequency support effects are consistent when $K_{p,\mathrm{GFM}} = 1/K_{p,\mathrm{GFL}}$. The difference of frequency nadirs is less than 0.005 Hz.

4.1.2. Case2: Synthetic inertia control (SIC) of GFL vs. VSG control of GFM

The results are shown in Fig. 10(c) and (d). Their frequency responses are the same when the virtual inertia coefficient K_{in} and the droop coefficient K_{dr} of SIC as well as the inertia coefficient J and the damping coefficient D of the VSG satisfy condition $K_{dr} = D, K_{in} = J$.

4.1.3. Case3: Optimal control of the GFL vs. proposed optimal control of the GFM

The results are shown in Fig. 10(e) and (f). Since the control parameters k_{wn} and T_{w} are set identically, only k_{wm} affects the frequency regulation effect. It can be seen from the illustration that the frequency support effect is consistent when $k_{\mathrm{wm,GFM}} = k_{\mathrm{wm,GFL}}$.

Table 1
The sub-item and overall proposed HOFS schemes used for validation in parts.

Scheme	Description
HOFS-GFM	The GFM optimal frequency support control of Level I in the HOFS scheme
HOFS-LI	The HOFS scheme without Level II of coordination.
HOFS	The proposed complete hierarchical optimal frequency support scheme.

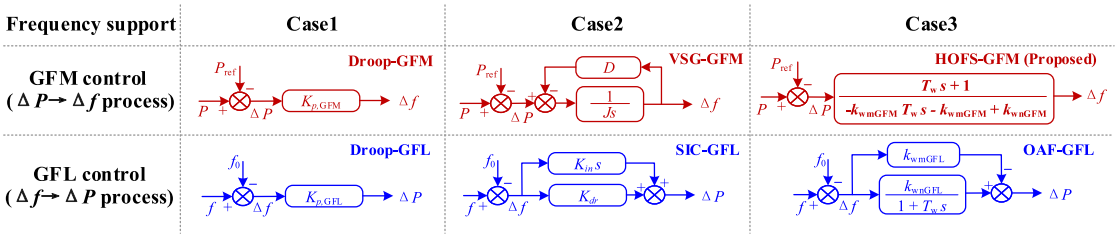

Fig. 9. Three frequency support control structures of GFM-WTs and GFL-WTs for duality consistency verification.

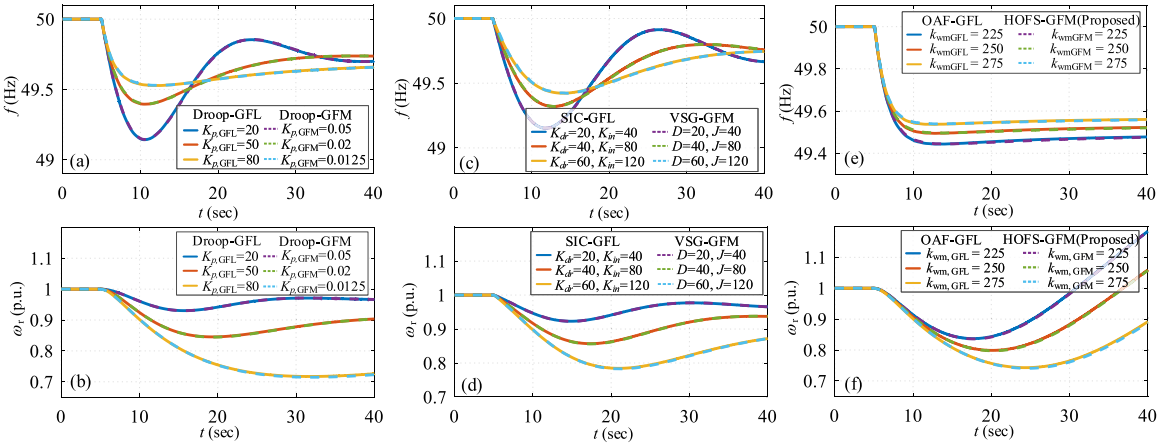

Fig. 10. Results for the dual frequency support of different GFM and GFL typical and proposed controls. (a) Frequency response (Droop-GFL and Droop-GFM). (b) Rotor speed (Droop-GFL and Droop-GFM). (c) Frequency response (SIC-GFL and VSG-GFM). (d) Rotor speed (SIC-GFL and VSG-GFM). (e) Frequency response (OAF-GFL and HOFS-GFM). (f) Rotor speed (OAF-GFL and HOFS-GFM).

In summary, the frequency support of the WTs is consistent once the GFL and GFM controls satisfy duality consistency. The GFM-WTs and GFL-WTs differ in the synchronization structure, especially the dynamics of the PLL in collecting frequency. It leads to a slight difference in the frequency support results. However, the difference in frequency nadir is less than 0.01 Hz from the simulation results. The effect is negligible. The inference of duality consistency is not only for the above cases. it holds for other GFM and GFL frequency support controls.

4.2. Validation of the GFM optimal frequency support control in HOFS scheme

Both stages of the GFM optimal control are applied in this subsection. This case verifies the effect of the proposed GFM optimal control and serves as a pre-calibration of the parameters. This work is carried out offline in advance, as in this case. Therefore, the common maximum load disturbance ΔP_d of 500 MW is used. The difference between the peak and low loads per day is more than 80% of the maximum load in the regions of Germany, Austrian and UK [40]. Therefore, a about 20% load increase during the load rise period is possible [41]. Specifically, a 500 MW load increase occurs at t = 5 s on bus 7 of the system. For the parameters setting, $k_{\mathrm{wn,sum}}$ = 480 and $T_{\mathrm{w},i}$ = 15 are set according to Section 3. The set value of $k_{\mathrm{wm,sum}}$ = 221 is obtained by Eq. (21) after a small amount of adjustment. From Section 4.1, the parameters setting can also be used for GFL optimal control. The results of the tests with this setting are shown in Fig. 11.

Due to the frequency deviation exceeding the deadband at t = 5.01 s, it enters into Stage I. The proposed HOFS-GFM is used to control the frequency to fall down quickly to the minimum value and keep it steady in Stage I. The rise in the active power over the mechanical power leads to a decrease in the rotor speed. The speeds reach the minimum 0.70 at t = 18.46 s but do not cross that, as shown in Fig. 11(b). The electromagnetic power $P_{\mathrm{eGFM},i} < P'_{\mathrm{MPPT},i}$ at t_r = 24.51 s. Therefore, the GFM optimal control is switched from Stage I to Stage II speed recovery. After that, the rotor speeds and frequency of the WTs recover simultaneously as shown in Fig. 8(a) and (c). Eventually, the frequency reaches a steady state value. The f_{nadir} of the whole process is 49.06 Hz using the proposed HOFS-GFM.

For comparison, the VSG-GFM is adopted with parameters employed based on maximizing the full kinetic energy of the WTs. As shown in Fig. 11(a), the frequency has a nadir of 48.92 Hz at t = 13.05 s. In addition, the f_{nadir} is 48.15 Hz without WF involvement in frequency support. The proposed HOFS scheme improves 49.19% in the f_{nadir} compared to the WF not participating in the frequency support and 12.96% compared to the VSG-GFM.

Therefore, the proposed HOFS scheme has a better frequency support effect in GFM mode compared to others. In addition, due to the smooth setting of the switching point, the frequency is also recovered during the speed recovery stage. That avoids an immediate secondary drop in frequency.

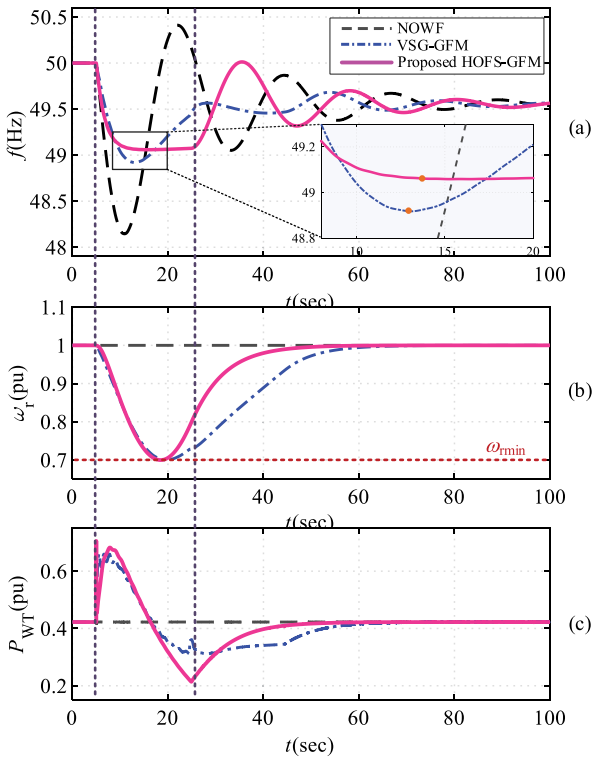

Fig. 11. Results of frequency support when the WTs are operating in GFM mode. (a) Frequency response. (b) Rotor speed. (c) Output active power.

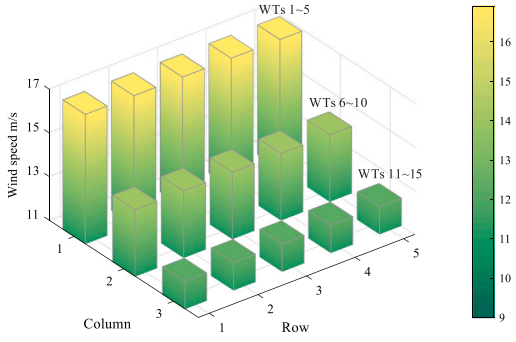

Fig. 12. Wind speed of WTs in the WF considering wake effects.

4.3. Validations of HOFS scheme at different wind speeds

To further validate the effectiveness of the proposed HOFS scheme at different wind speeds, specific operating conditions are set. The wind direction is forward to WTs 1~5. The results of the distribution of wind speeds in the case studies are obtained by Eqs. (25)–(28). The specific parameters of the wind farm are shown in Table 3.

4.3.1. Case1: High wind speed scenario

The wind speed of the WF is set to be 16.9 m/s. The WTs 1~5 are operated in the constant speed zone as B-C in Fig. 6(b). Due to the wake effect, WTs 6~15 have slightly lower wind speeds. The wind speed distribution of the WF according to [38] is shown in Fig. 12. The disturbance is the same as that set in Section 4.2.

Using the proposed HOFS scheme, the frequency and the output power of the WTs are shown in Fig. 13(a) and (b), respectively. In order to verify the role of Level II of coordination, HOFS-LI is also demonstrated. The power output of WTs 1~5 is limited from t = 5.92 s due to exceeding the power limitation. This results in part of the power failed to be generated. f_{nadir} is 49.05 Hz using HOFS-LI. The role of coordination control is clearly shown in Fig. 13. The power failed to be generated by WTs 1~5 is augmented by WTs 6~11 through the power interaction factor x_i. This is due to the fact that the medium wind speed WTs have sufficient margins away from the power and rotor speed limitations. The WTs 6~10 augment the power and they make better use of the rotor kinetic energy with a minimum speed of 0.702.

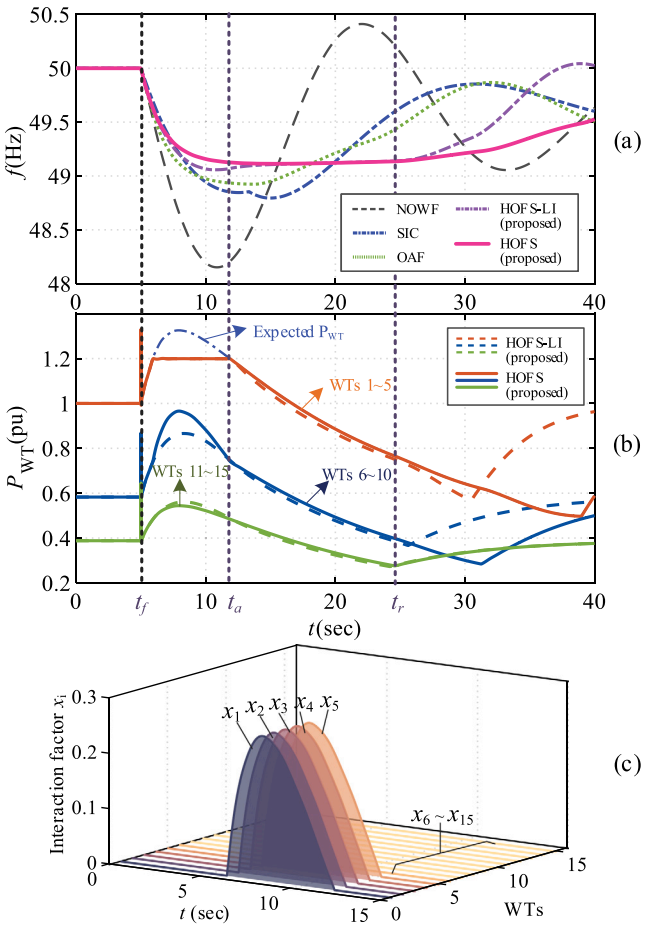

Fig. 13. Results for frequency support of the WF at high wind speed (a) Frequency response under different controls. (b) Output power of WTs. (c) Interaction factors.

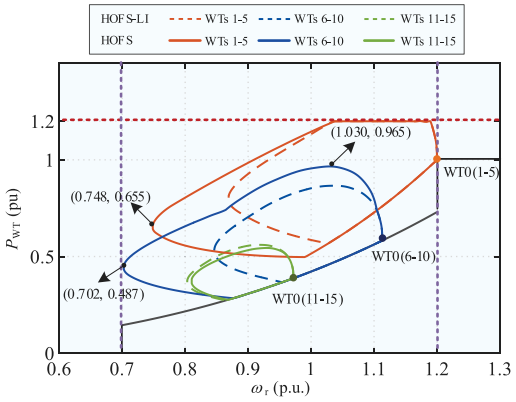

Fig. 14. Power-speed trajectories of WTs in the WF using proposed scheme.

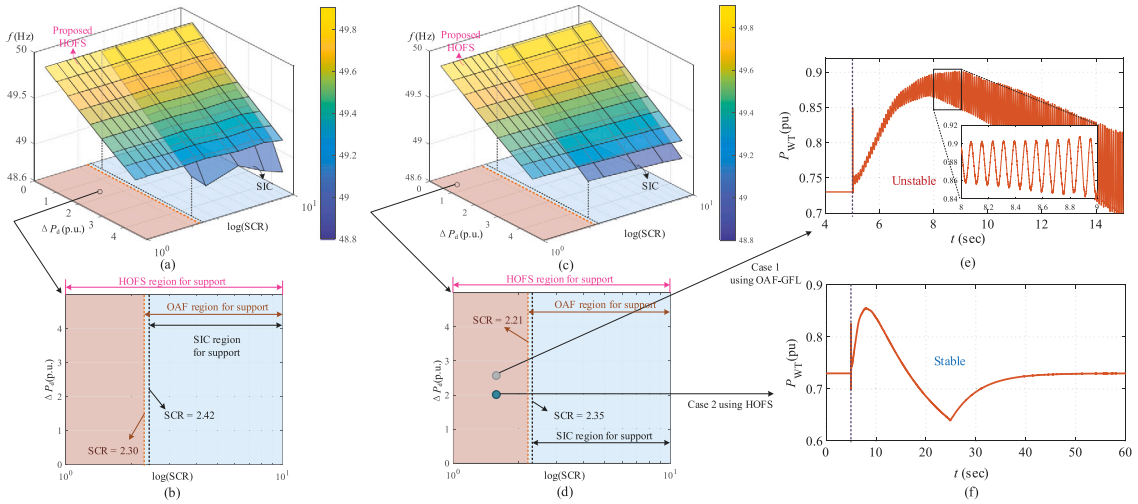

Fig. 15. Results of traversal tests for the WF with different SCR and disturbances. (a) Frequency support effects (traversal test 1). (b) Support regions (traversal test 1). (c) Frequency support effects (traversal test 2). (d) Support regions (traversal test 2). (e) Case 1 using SIC control (SCR = 1.6). (f) Case 2 using HOFS scheme (SCR=1.6).

Moreover, that indirectly results in WTs 1~5 also making better use of the kinetic energy in the following period, with a minimum speed of 0.748. Hence, f_{nadir} is raised to 49.11 Hz.

Comparative experiments of other controls are carried out. The f_{nadir} is 48.15 Hz without the WF support. In particular, the centralized SIC control and OAF [30] are used in the unconventional scenario of high wind speed. Using SIC control, a few WTs undergo the rotor speed below 0.7 at t = 13.34 s limited by the wind speed resource differences between WTs. They enter rotor speed protection. It leads to a second drop in frequency with f_{nadir} = 48.79 Hz. Using OAF control [30], the frequency is unable to be maintained at the nadir according to the expected characteristics. It has a frequency nadir of 48.92 Hz. The results of these two controls are poor due to the fact that the relationship between power and speed in the constant speed zone is different from that in the MPPT zone.

As a result, the proposed HOFS scheme enables the WF to support the frequency at high wind speed scenario with an improvement of 26.4% and 17.6% in f_{nadir} compared to the SIC and OAF controls, respectively.

4.3.2. Case2: Medium-low wind speed scenario

The wind speed of the WF is set to be 12.5 m/s. Wind speed of each WT considering wake effects: [12.50, 12.50, 12.50, 12.50, 12.50; 10.39, 10.39, 10.39, 10.39, 10.39; 9.14, 9.14, 9.14, 9.14, 9.14]. All WTs are operated in the MPPT zone as A-B in Fig. 6(b). A 250 MW load increase occurs at t = 5 s on bus 7. f_{nadir} is 49.04 Hz if the WF does not support it. Using the SIC control, the f_{nadir} is enhanced to 49.53 Hz. By contrast, a similar f_{nadir} = 49.53 Hz is obtained using OAF control or the proposed HOFS scheme.

4.4. Frequency support effects under different grid strengths

To verify the adaptability of the proposed scheme under different grid strengths, traversal tests are carried out. The traversal settings include (a) grid strengths SCR from 1.0 to 10. (b) load surge disturbances from 50 to 450 MW. The frequency support results of the proposed scheme and other controls with the above settings are shown in Fig. 15.

4.4.1. Traversal test 1

Wind speed of 14 m/s with 10° direction angle is set. Wind speed of each WT considering wake effects: [14.00, 14.00, 14.00, 14.00, 14.00; 14.00, 12.37, 12.37, 12.37, 12.37; 14.00, 12.27, 12.23, 12.23, 12.23]. Fig. 15(a) and (b) show the results of the frequency nadir and the support regions for several controls. For the support regions, SIC control and OAF control [30] are available for frequency support under SCR > 2.42 and SCR > 2.30, respectively. Otherwise, the oscillations will occur leading to instability. This is due to the weak stability of the GFL-WTs under the weak grid. Thus the support regions of SIC control and OAF control are SCR = 2.42~10 and SCR = 2.30~10, respectively. Using the proposed HOFS scheme, the stability is excellent under the extremely weak grid with the lowest operating SCR of 1.0. As a result, the minimum operating SCR is improved from 2.3 to 1.0. For the support of f_{nadir}, the HOFS scheme improves 16.3% on average compared to the SIC control.

4.4.2. Traversal test 2

Wind speed of 16.5 m/s with 10° direction angle is set. Wind speed of each WT considering wake effects: [16.50, 16.50, 16.50, 16.50, 16.50; 16.50, 14.57, 14.57, 14.57, 14.57; 16.50, 14.45, 14.41, 14.41, 14.41]. Fig. 15(c) and (d) show the results of the frequency nadir and the support regions for several controls. For the support regions, the different wind speed affects the critical SCR a little bit. SIC control and OAF control are available for frequency support under SCR > 2.35 and SCR > 2.21, respectively. Thus their support regions are SCR = 2.35~10 and SCR = 2.21~10, respectively. With the proposed HOFS scheme, the minimum operating SCR is 1.0. As a result, the minimum operating SCR is improved from 2.21 to 1.0. For the support of f_{nadir}, the HOFS scheme improves 18.5% on average compared to the SIC control.

The cases under extremely weak grid are demonstrated as in Fig. 15(e) and (f). Case 1 illustrates the response of the OAF control suffering from a 200MW disturbance at SCR = 1.6. Fig. 15(e) shows the active power output of WT_1. The occurrence of oscillation dispersion indicates that the system cannot operate stably. As a comparison, Case 2 shows the response results of the proposed HOFS scheme with similar settings. The output active power of WT_1 is generated correctly to support the frequency as shown in Fig. 15(f).

Observing the frequency support effects under different load perturbations, the enhancement percentile of the proposed scheme is almost unaffected by more than 12% compared to other methods. Therefore, the proposed scheme is better in terms of frequency support at different load disturbance sizes.

4.5. Comparative analysis of frequency time-domain characteristics and stability

To quantitatively demonstrate the frequency support effects and advantages of the proposed scheme, we compare the time-domain characteristics of the frequency and stability under different controls in

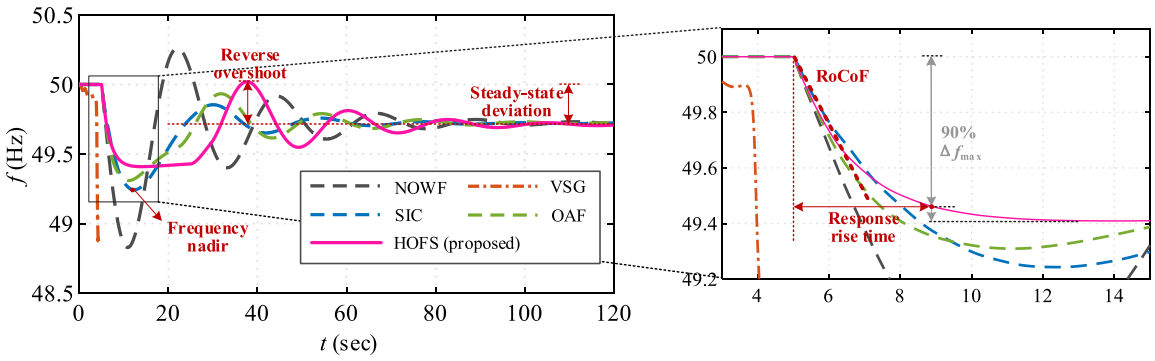

Fig. 16. Results of the frequency responses in the scenario of strong grid and high wind speed in the Table 2.

several aspects. The compared frequency time-domain characteristics include the maximum rate of change of frequency (RoCoF), response rise time, nadir, reverse overshoot, and steady-state deviation. Moreover, these comparison cases are carried out in three typical scenarios, including high as well as low wind speeds and strong as well as weak grids. The system suffers a 300 MW power disturbance at $t = 5$ s. The time-domain characteristics of the frequency under different controls are shown in Table 2. As an example of the scenario of strong grid and high wind speed in the Table 2, the results of the frequency responses over a long period of time are shown in Fig. 16.

The characteristics and advantages of the proposed HOFS are shown by comparison:

- It has an excellent frequency nadir and response speed, although there is a slight loss in RoCoF and reverse overshoot. The frequency support in different scenarios reaches over 49% improvement compared to NOWF, all with the best frequency nadir. In terms of losses, there is about a 20% loss in RoCoF in the initial period and a slight boost in reverse overshoot, but these are still acceptable.
- It has the same effect of steady-state deviation in the later period of the frequency support. This is due to the fact that the wind farms are finally restored to the MPPT operating point without additional active power supply.
- It works for both strong and weak grid scenarios. As a comparison, all other controls have oscillations leading to instability in a certain type of scenario.

4.6. Validation of effectiveness in low-inertia large systems

To verify the effectiveness of the scheme in a low-inertia large system, a improved New England 39-bus system is built and tested. The New England power system consists of 10 synchronous generators, 39 buses and 46 branches. The constructed improved system replaces 4 synchronous generators G2, G3, G4, G6 with 4 wind farms. Each wind farm consists of five 100 MW equivalent wind turbines. The proportion of wind power in this system amounts to 40.37%. The whole system is a low-inertia grid. The structure of the system is shown in Fig. 17. Compared to a conventional power system, a low-inertia grid induces a larger frequency change for a perturbation. With the proposed HOFS scheme, one WT in each wind farm is set to GFM type.

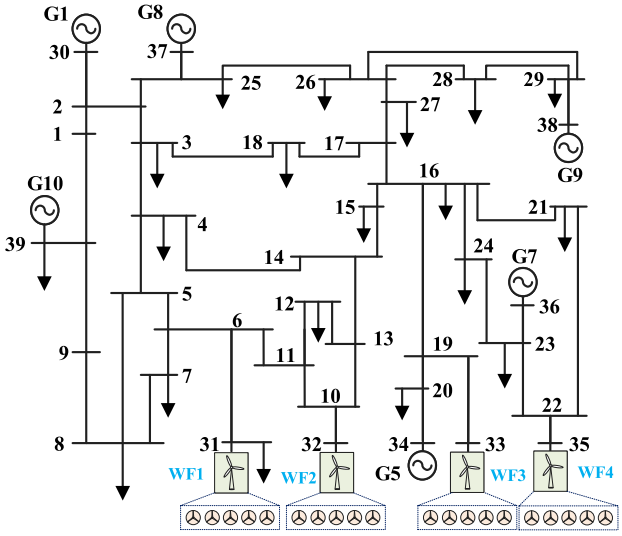

Fig. 17. The structure of improved New England 39-bus system with 4 wind farms.

A disturbance example is a sudden increase in load of 600 MW on bus 39 at t = 1s. Using the proposed HOFS scheme, Fig. 18 illustrates the active power output of each turbine at two moments. They correspond to the frequency decline support stage and the rotor speed

Table 2
Time-domain characteristics of frequency under different controls.

Scenarios	Controls	RoCoF (Hz/s)	Response rise time (s)	Nadir (Hz)	Reverse overshoot (Hz)	Steady-state deviation (Hz)	Support effect of the nadir	Stability
Weak grid	SIC	——	——	——	——	——	——	Unstable
(SCR = 1.5)	VSG	0.240	5.05	49.34	**0.19**	0.27	42.11%	Stable
Low wind speed	OAF	——	——	——	——	——	——	Unstable
(12.5 m/s)	HOFS	0.297	**3.25**	**49.46**	0.20	0.27	52.63%	**Stable**
Weak grid	SIC	——	——	——	——	——	——	Unstable
(SCR = 1.5)	VSG	**0.250**	4.74	49.25	**0.14**	0.27	33.04%	Stable
High wind speed	OAF	——	——	——	——	——	——	Unstable
(16.5 m/s)	HOFS	0.292	**3.54**	**49.47**	0.29	0.27	**52.68%**	**Stable**
Strong grid	SIC	**0.256**	4.71	49.24	**0.13**	0.28	35.59%	Stable
(SCR = 10)	VSG	——	——	——	——	——	——	Unstable
High wind speed	OAF	0.314	**3.44**	49.31	0.21	0.28	41.53%	Stable
(16.5 m/s)	HOFS	0.313	3.69	**49.41**	0.30	0.28	**49.98%**	**Stable**

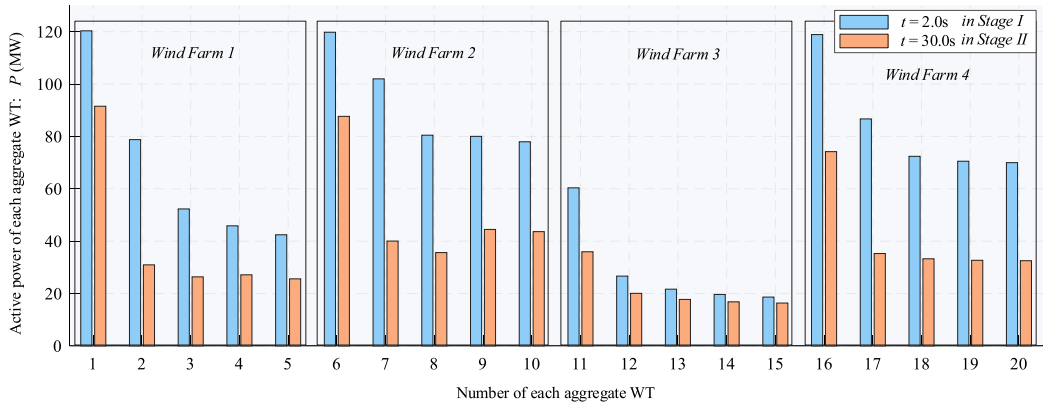

Fig. 18. The active power output of each equivalent WT at two specific moments in the frequency regulation process using HOFS scheme.

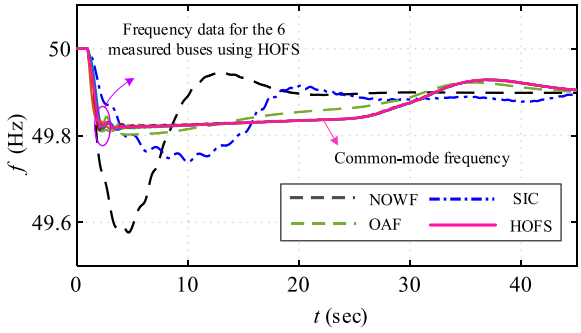

Fig. 19. Frequency dynamics under different controls in the case of the improved New England 39 bus system.

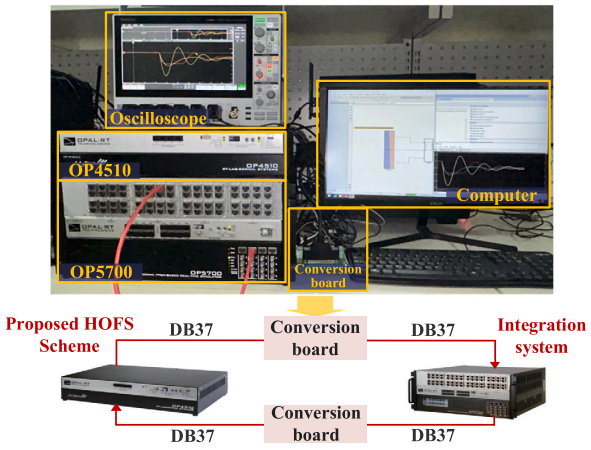

Fig. 20. Opal-RT real-time experimental platform.

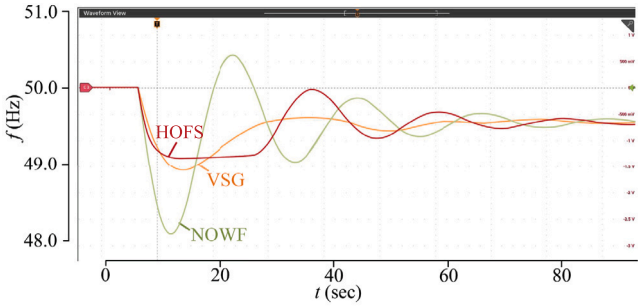

Fig. 21. Frequency response results of a 500 MW load increase on bus 7 using different schemes in Opal-RT.

recovery stage, respectively. The dynamics of frequency under various controls are shown in Fig. 19. If none of the four wind farms are involved in regulation, the frequency nadir is 49.58 Hz. The frequency nadir with SIC control and OAF control is 49.74 Hz and 49.79 Hz, respectively. By contrast, the HOFS scheme can support the frequency nadir up to 49.82 Hz. Therefore, the effectiveness of the proposed scheme in low-inertia large systems is verified.

This paper focuses on control design involving coordination within a single wind farm. Coordination between multiple wind farms in large systems will be considered in future studies.

4.7. Real-time experimental verification

To further verify the effectiveness of the proposed HOFS scheme by experiments, the Opal-RT real-time simulation platform is constructed as shown in Fig. 20. It consists of OP4510 and OP5700. The interconnected system of the experimental simulation is consistent with the example system in Fig. 8. The wind farm integration system is set up in the OP5700 simulator, while the HOFS scheme is established in OP4510 simulator. The two simulators are connected to each other through a conversion board and DB37 signal lines. Frequency deviation and active power will be transmitted from both simulators via the DB37.

Experimental verification at rated operating condition: The frequency response results of Section 4.2 on the Opal-RT platform are shown in Fig. 21. The f_{nadir} using the HOFS scheme is 49.06 Hz. The results confirm the superiority of the proposed HOFS scheme for frequency nadir support when adopting the GFM optimal frequency support control.

Experimental validation at different wind speeds: To verify the feasibility of the scheme at different wind speeds, the results of the proposed HOFS scheme are verified in experiments for different wind speed cases in Section 4.2 for each wind speed. As shown in Fig. 22(a), compared with the methods of VSG and OAF, the frequency support of the proposed control scheme is significantly better. Secondly, the dynamics of the system frequency was observed by an oscilloscope at a wind speed of 12.5 m/s. According to Fig. 22(c), the proposed HOFS scheme has a better frequency nadir compared to other controls. Its effect is close to but still better than the OAF method.

Obviously, the experimental results in Fig. 22 are consistent with the related simulation results in Fig. 14. Therefore, the Opal-RT real-time simulation platform further verifies the effectiveness of the proposed scheme and the simulation results.

Experimental validation at extreme weak grids: To further the feasibility of the proposed scheme in extreme scenarios, experiments were conducted under weak grids. The conducted experiments are under an extreme weak grid (SCR = 1.6). The frequency response and the active

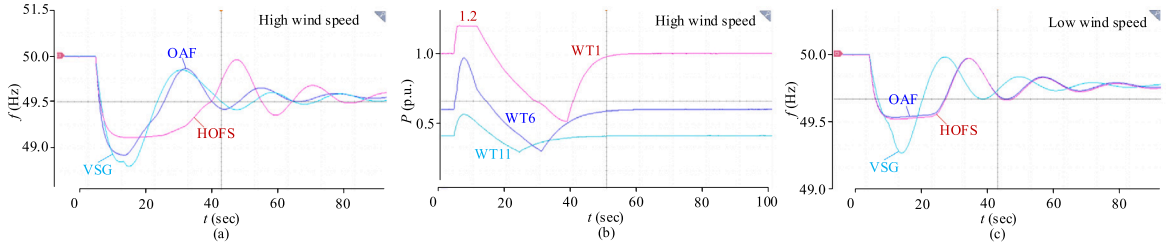

Fig. 22. Experimental results of the proposed scheme based on Opal platform at different wind speeds. (a) Frequency response results at high wind speed (16.5 m/s). (b) Turbine power at high wind speed (16.5 m/s). (c) Frequency response results at low wind speed (12.5 m/s).

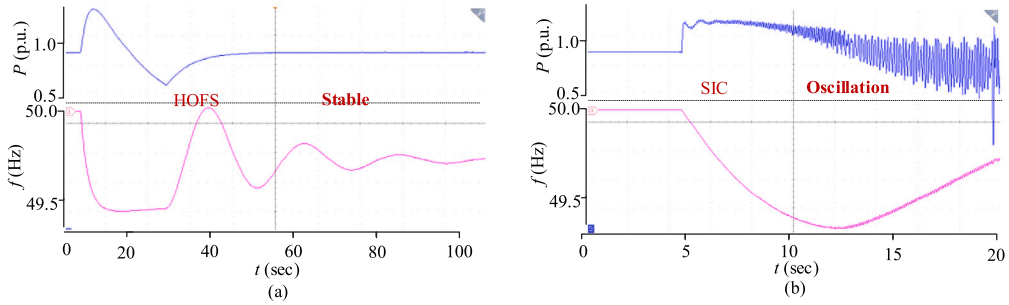

Fig. 23. Experimental results of the proposed scheme based on the Opal-RT platform under an extreme weak grid. (a) Frequency and active power dynamics of the proposed HOFS. (b) Frequency and active power dynamics under SIC control.

power of representative WT using the HOFS scheme on the Opal-RT platform are shown in Fig. 23(a). As a comparison, the experimental results of SIC are shown in Fig. 23(b). The oscilloscope results show that the proposed scheme is able to support frequency nadir with 49.43 Hz in an extreme weak grid. However, the power of the wind farm using SIC control appears to oscillate and the system is unstable. Therefore, the experiments verify the superiority of the proposed scheme in extreme conditions.

5. Conclusion

This paper proposes a hierarchical optimal frequency support scheme for the hybrid WF with both GFM-WTs and GFL-WTs. To obtain the scheme, this paper reveals the duality consistency of the GFM-WTs and GFL-WTs in terms of frequency support by establishing GFM-SFR and GFL-SFR models at first. The inference that the frequency support effects of GFM-WTs and GFL-WTs are consistent once both structures and parameters satisfy the revealed duality consistency formula is of generality. Specifically, the results of the three dual controls as (1) Droop-GFL and Droop-GFM, (2) SIC-GFL and VSG-GFM, and (3) OAF-GFL and HOFS-GFM (Proposed) confirm the finding in the case studies. Based on this, the HOFS scheme is proposed. Its main purpose is to achieve optimal frequency support of the WF over a wide range of grid strength. The proposed scheme consists of two levels: optimal frequency control of WT and coordination control of multiple WTs. The validation results of a two-area integration system with a wind farm in MATLAB/Simulink and Opal-RT experimental platform are presented and analyzed. The results show that the proposed HOFS scheme is capable of operating and realizing frequency support at SCR from 1.0 to 10. It is a significant improvement over the existing controls of the WF with a minimum SCR of about 2.2. It works for both strong and weak grid scenarios. In addition, the frequency regulation effectiveness of the proposed scheme is excellent, with an improvement of more than 12% in frequency nadir compared to controls such as SIC and VSG although there is a slight loss in RoCoF. The advantage of such frequency support is more obvious in high wind speed scenarios with more than 19% improvement.

CRediT authorship contribution statement

Qihang Zong: Writing – original draft, Visualization, Methodology, Investigation, Data curation. **Wei Yao:** Writing – review & editing, Supervision, Conceptualization. **Hongyu Zhou:** Writing – review & editing, Data curation. **Yongxin Xiong:** Investigation, Writing – review & editing. **Wei Gan:** Writing – review & editing, Supervision. **Jinyu Wen:** Supervision.

Declaration of competing interest

The authors declare that they have no known competing financial interests or personal relationships that could have appeared to influence the work reported in this paper.

Acknowledgments

This work was supported by National Key R&D Program of China (No. 2022YFB4202304).

Appendix

Detailed formulas of downstream WT wind speed affected by wake effect are:

$$V_j = V_0\left[1 - \sum_{i=1}^{n}\left(1 - \sqrt{1 - C_{T,i}}\right)\cdot \xi_{ij}\right] \tag{25}$$

$$\xi_{ij} = \left(\frac{r_0}{r_i}\right)^2 \frac{A_s}{A_0} \tag{26}$$

$$r_i = r_0 + x_{ij}\cdot \tan\alpha \approx r_0 + x\cdot\alpha \tag{27}$$

$$A_s = {r_i}^2\cos^{-1}\left(\frac{L_{ij}}{r_i}\right) + r_0^2\cos^{-1}\left(\frac{d_{ij} - L_{ij}}{r_i}\right) - d_{ij}z_{ij} \tag{28}$$

where, r_0 is the radius of WT and x is the distance between the upstream WT and the downstream WT. A_0 is the sweep area of WT. The downstream WT is partly shadowed by the upstream WT. A_s is the shadowed area. Radius r_i describes the expansion effect of the

Table 3
Parameters of the wind farm.

Parameters and description		Value
Geographic distribution of WF	Distance between columns $x_{ij,1}$ (m)	600
	Distance between columns $x_{ij,2}$ (m)	300
	Distance between rows d_{ij} (m)	400
Parameters of WT	Decay coefficient α (p.u.)	0.05
	Thrust coefficient $C_{T,i}$ (p.u.)	0.588
	Radius of WT r_0 (m)	65.5

wake. The affected area in downstream increases according to decay coefficient α. $C_{T,i}$ is the thrust coefficient.

Data availability

The authors do not have permission to share data.

References

[1] Han R, Hu Q, Fang X, Qian T, Zhang Y. Frequency security-constrained unit commitment with fast frequency support of DFIG-based wind power plants. Int J Electr Power Energy Syst 2024;160:110119.

[2] Han S, He M, Zhao Z, Chen D, Xu B, Jurasz J, et al. Overcoming the uncertainty and volatility of wind power: Day-ahead scheduling of hydro-wind hybrid power generation system by coordinating power regulation and frequency response flexibility. Appl Energy 2023;333:120555.

[3] Gao H, Zhang F, Ding L, Cornélusse B, Zhang G, Salimu A. Multi-segment droop control and optimal parameter setting strategy of wind turbine for frequency regulation. Int J Electr Power Energy Syst 2024;158:109968.

[4] Han F, Zhang X, Li M, Li F, Zhao W. Stability control for grid-connected inverters based on hybrid-mode of grid-following and grid-forming. IEEE Trans Ind Electron 2024;71(9):10750–60.

[5] Li M, Zhang X, Guo Z, Pan H, Ma M, Zhao W. Impedance adaptive dual-mode control of grid-connected inverters with large fluctuation of SCR and its stability analysis based on D-partition method. IEEE Trans Power Electron 2021;36(12):14420–35.

[6] Huang L, Xin H, Li Z, Ju P, Yuan H, Wang G. Identification of generalized short-circuit ratio for on-line stability monitoring of wind farms. IEEE Trans Power Syst 2020;35(4):3282–5.

[7] Henderson C, Egea-Alvarez A, Xu L. Analysis of optimal grid-forming converter penetration in AC connected offshore wind farms.

[8] Wang G, Lyu J, Rao Y. Small-signal stability analysis of hybrid wind farm with grid-following and grid-forming wind turbine generators. In: 2023 IEEE pELS students and Young professionals symposium. 2023, p. 1–6.

[9] Kim J-S, Kim Y-J, Gomis-Bellmunt O. Optimal frequency regulation of multi-terminal HVDC-linked grids with deloaded offshore wind farms control. IEEE Trans Sustain Energy 2024;15(1):290–303.

[10] Jiang C, Cai G, Yang D, Liu X, Hao S, Li B. Multi-objective configuration and evaluation of dynamic virtual inertia from DFIG based wind farm for frequency regulation. Int J Electr Power Energy Syst 2024;158:109956.

[11] Huang S, Wu Q, Liao W, Wu G, Li X, Wei J. Adaptive droop-based hierarchical optimal voltage control scheme for VSC-HVDC connected offshore wind farm. IEEE Trans Ind Electron 2021;17(12):8165–76.

[12] Yang D, Wang X, Yan G-G, Jin E, Huang J, Zheng T, et al. Decoupling active power control scheme of doubly-fed induction generator for providing virtual inertial response. Int J Electr Power Energy Syst 2023;149:109051.

[13] Boyle J, Littler T, Muyeen S, Foley AM. An alternative frequency-droop scheme for wind turbines that provide primary frequency regulation via rotor speed control. Int J Electr Power Energy Syst 2021;133:107219.

[14] Zhang H, Xiang W, Lin W, Wen J. Grid forming converters in renewable energy sources dominated power grid: Control strategy, stability, application, and challenges. J Mod Power Syst Clean Energy 2021;9(6):1239–56.

[15] Ravanji MH, Zhou W, Mohammed N, Bahrani B. Comparative analysis of the power output capabilities of grid-following and grid-forming inverters considering static, dynamic, and thermal limitations. IEEE Trans Power Syst 2024;39(2):2693–705.

[16] Ma Q, Chen L, Li L, Min Y, Gong Y, Liang K. Effect of grid-following VSC on terminal frequency. IEEE Trans Power Syst 2023;38(2):1775–8.

[17] Du W, Wang X, Wang H. Sub-synchronous interactions caused by the PLL in the grid-connected PMSG for the wind power generation. Int J Electr Power Energy Syst 2018;98:331–41.

[18] Li Y, Gu Y, Green TC. Revisiting grid-forming and grid-following inverters: A duality theory. IEEE Trans Power Syst 2022;37(6):4541–54.

[19] Pattabiraman D, Lasseter R, Jahns T. Comparison of grid following and grid forming control for a high inverter penetration power system. In: Proc IEEE power energy soc gen meeting. 2018, p. 1–5.

[20] Cheng Y, Azizipanah-Abarghooee R, Azizi S, Ding L, Terzija V. Smart frequency control in low inertia energy systems based on frequency response techniques: A review. Appl Energy 2020;279:115798.

[21] Tang Y, Yang P, Yang Y, Zhao Z, Lai LL. Fuzzy adaptive frequency support control strategy for wind turbines with improved rotor speed recovery. IEEE Trans Sustain Energy 2024;15(2):1351–64.

[22] Ghosh S, Kamalasadan S, Senroy N, Enslin J. Doubly fed induction generator (DFIG)-based wind farm control framework for primary frequency and inertial response application. IEEE Trans Power Syst 2015;31(3):1861–71.

[23] Lee J, Muljadi E, Srensen P, Kang YC. Releasable kinetic energy-based inertial control of a DFIG wind power plant. IEEE Trans Sustain Energy 2016;7(1):279–88.

[24] Díaz-González F, Hau M, Sumper A, Gomis-Bellmunt O. Participation of wind power plants in system frequency control: Review of grid code requirements and control methods. Renew Sust Energ Rev 2014;34:551–64.

[25] Bao W, Ding L, Kang YC, Sun L. Closed-loop synthetic inertia control for wind turbine generators in association with slightly over-speeded deloading operation. IEEE Trans Power Syst 2023;38(6):5022–32.

[26] Yao Y, Yao W, Xiong Y, Lin S, Zhou H, Wen J, et al. Distributed adaptive leaderless consensus control of wind farm for fast frequency support. IEEE Trans Ind Electron 2024;71(10):12255–66.

[27] Meng X, Liu J, Liu Z. A generalized droop control for grid-supporting inverter based on comparison between traditional droop control and virtual synchronous generator control. IEEE Trans Power Electron 2019;34(6):5416–38.

[28] Soni N, Doolla S, Chandorkar MC. Improvement of transient response in microgrids using virtual inertia. IEEE Trans Power Deliv 2013;28(3):1830–8.

[29] Sun M, Xu F, Chen L, Min Y, Tian Z. Optimal auxiliary frequency control strategy of wind turbine generator utilizing rotor kinetic energy. Proc CSEE 2021;41(2):506–14.

[30] Sun M, Sun Y, Chen L, Zou Z, Min Y, Liu R, et al. Novel temporary frequency support control strategy of wind turbine generator considering coordination with synchronous generator. IEEE Trans Sustain Energy 2022;13(2):1011–20.

[31] Krpan M, Kuzle I. Introducing low-order system frequency response modelling of a future power system with high penetration of wind power plants with frequency support capabilities. IET Renew Power Gener 2018;12(13):1453–61.

[32] Gao H, Xin H, Huang L, Li Z, Huang W, Wu C, et al. Common-mode frequency in converter-integrated power systems: Definition, analysis, and quantitative evaluation. IEEE Trans Power Syst 2022;37(6):4846–60.

[33] Shen J, Li W, Liu L, Jin C, Wen K, Wang X. Frequency response model and its closed-form solution of two-machine equivalent power system. IEEE Trans Power Syst 2020;36(3):2162–73.

[34] Ma S, Geng H, Yang G, Pal BC. Clustering-based coordinated control of large-scale wind farm for power system frequency support. IEEE Trans Sustain Energy 2018;9(4):1555–64.

[35] González-Longatt F, Wall P, Terzija V. Wake effect in wind farm performance: Steady-state and dynamic behavior. Renew Energy 2012;39(1):329–38.

[36] Lin S, Yao W, Xiong Y, Zhao Y, Shi Z, Ai X, et al. MatPSST: A matlab/simulink-based power system simulation toolbox for research and education. IET Gener Transm Distrib 2023;17(10):2272–88.

[37] Xin H, Liu C, Chen X, Wang Y, Prieto-Araujo E, Huang L. How many grid-forming converters do we need? A perspective from small signal stability and power grid strength. IEEE Trans Power Syst 2024.

[38] Lyu X, Jia Y, Dong Z. Adaptive frequency responsive control for wind farm considering wake interaction. J Mod Power Syst Clean Energy 2021;9(5):1066–75.

[39] Hu Z, Gao B, Mao Y. Nonlinear model predictive control-based active power dispatch strategy for wind power plant considering dynamic wake effect. Int J Electr Power Energy Syst 2023;148:108996.

[40] Anvari M, Proedrou E, Schäfer B, Beck C, Kantz H, Timme M. Data-driven load profiles and the dynamics of residential electricity consumption. Nature Commun 2022;13(1):4593.

[41] Kheshti M, Ding L, Bao W, Yin M, Wu Q, Terzija V. Toward intelligent inertial frequency participation of wind farms for the grid frequency control. IEEE Trans Ind Inf 2019;16(11):6772–86.